Research article

Multi-dimensional switched reluctance motors for industrial applications

J.F. Pan
College of Mechatronics and Control Engineering, Shenzhen University, Shenzhen, China, and

Norbert Cheung
Hong Kong Polytechnic University, Kowloon, Hong Kong

Abstract

Purpose – The paper aims to discuss a new direction of design outline of four-axis machine with multi-dimensional motors. It proposes an integrated, direct-drive machine based on switched reluctance (SR) principles. This includes how the machine is constructed and the structure of each axis of motion. The simulation and control results are also provided for performance prediction. The study aims to provide a solution and find applications for high-performance, low-cost manufacturing facilities.

Design/methodology/approach – The study is based on simulation and experimental results for performance prediction of the multi-dimensional motors. With the approach of grounded theory on SR machines, design and construction of each axis of motion is verified with finite element analysis. Then, corresponding control strategy is provided for the control of each axis of motion. Some corresponding experimental results are carried out to verify motor performance.

Findings – The paper provides a general design procedure for direct-drive, integrated, multi-dimensional SR motors. It suggests a mechanically robust, low-cost and simple machine structure for potential applications of industrial multi-axis machines.

Research limitations/implications – Considering the performance from the prototype, it is expected to find applications in low-level force and torque output such as automated small-scale printed circuit board drillings.

Practical implications – Owing to the limitations of the present study, the machine needs further control tests for robust or adaptive applications. Therefore, researchers are encouraged to implement further advanced control strategies on the machine.

Originality/value – The authors attempt to provide a comprehensive solution of multi-axis machine design based on direct-drive, low-cost multi-dimensional SR motors.

Keywords Magnetic devices, Actuators, Finite element analysis

Paper type Research paper

Introduction

In high-precision process, to achieve high-precision 4D motions, most high-performance manufacturing machines apply a geared θ-axis head and a three-axis table for the X-, Y- and Z-axis. The multi-dimensional table often employs DC or AC motors as the prime motion actuators and couple their output shafts to mechanical motion translators (e.g. reduction gear, belt, ball screw, etc.) with mechanical slides, stacked on top of each other. The control for each axis of this type of machine is relatively easy since the rotary actuators are often based on stepping or servo motors. However, this type of machine has the disadvantages of complex mechanical structure, frequent mechanical adjustments, high manufacturing and maintenance cost and low reliability. Such disadvantages inherent in four-axis machines often indirectly lead to high cost of these machines (Cheung and Pan, 2003).

For a typical printed circuit board (PCB) drilling machine as its structure shown in Figure 1(a), two rotary motors are involved for θ and Z-axis of movement, respectively. The Z-axis motor couples a rotary-to-linear translator such as a lead screw mounted on Z-axis moving platform, integrated with a θ-axis motor responsible for drilling. Since the Z-axis motor needs to bear the whole weight of the moving platform and the θ-axis motor, in order to improve performance with less maintenance, measures should be taken for weight alleviation such as employing a pair of springs to support the Z-axis platform simultaneously. The typical structure of one

The current issue and full text archive of this journal is available at **www.emeraldinsight.com/0143-991X.htm**

Industrial Robot: An International Journal
38/4 (2011) 419–428

[DOI 10.1108/01439911111132102]

The authors would like to thank the Hong Kong Research Grants Council for the sponsoring of this research project under the project code PolyU 5140/07E and PolyU project under account code A-PH45; the authors would also like to thank Guangdong Natural Science Fund 2008225 and Shenzhen Government Fund 08cxy-29 for their support.

Figure 1 Typical structure of a four-axis PCB drilling machine

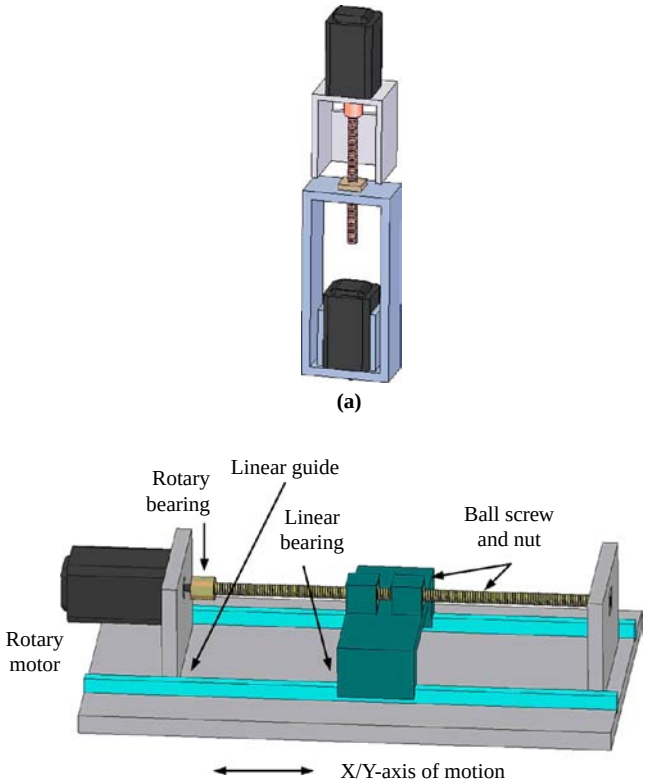

Notes: (a) θ- Z axis; (b) *X*- *Y* axis

axis for linear motion for X-Y moving platform that holds the work piece is shown in Figure 1(b). The X- or Y-axis of motion is realized by a rotary motor with ball screws and nuts and two axes are achieved with two such mechanisms vertically stacked on top of each other. As can be concluded, the machine structure with mechanical couplers may lead to inaccuracies and performance deteriorations due to coupler alignment, the manufacture imperfections of the mechanical couplers and the coupling between all components, etc. Moreover, the manufacture and maintenance cost is relatively expensive since most of the increase in cost goes to high-precision mechanical components, alignment procedure and maintenance effort.

In this paper, the authors intend to propose an integrated, direct-drive, four-axis machine based on multi-dimensional switched reluctance (SR) motors to eliminate complex mechanical translators and couplers. With the previous invention and development of a direct-drive planar SR motor (Cheung *et al.*, 2007), we intend to integrate an SR rotary-linear motor to form a direct-drive, four-axis PCB drilling machine prototype as shown in Figure 2.

The main advantages of applying SR principle for all axes of motion can be summarized as follows:

1 The motors have simple and robust mechanical structure with low inertia and direct-drive capability, therefore particular suitable for high-speed and high-precision applications.
2 Manufacturing of the motors are simple since rotor, mover and stators are all made from laminated silicon-steel sheets and there are no expensive or hard-to-handle materials such as the permanent magnet and commutator involved.
3 No mechanical transformer or couplers are required and the degree of precision is inherent to the structure and also special adjustments or alignments are unnecessary.
4 Compared with four-axis machine based on other motor principles, the proposed machine has a much simpler structure and is less expensive. It is also more robust and fault-tolerant with less over-heating problems.

Figure 2 The proposed θ-*Z* to *X*-*Y* machine

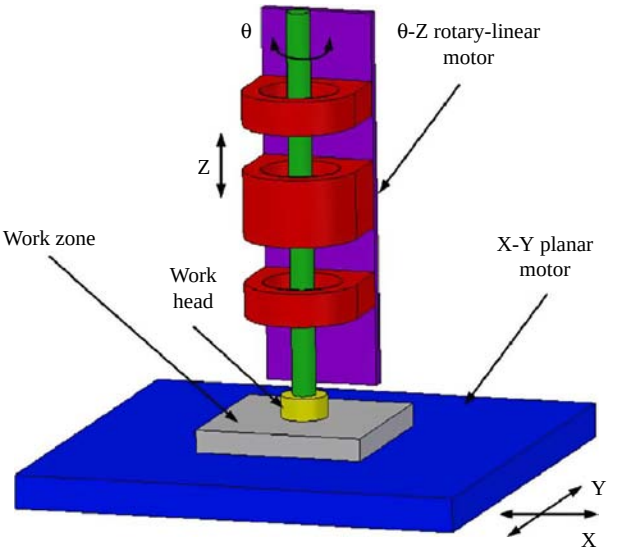

Considering all features of SR principle, the authors propose an integrated four-axis machine with the X-Y planar motor and the θ-*Z* rotary-linear motor. The design idea is based on the fact that it is always more effective to achieve complex motion requirements by software than mechanical hardware with the aid of fast development of power electronic techniques. The structure of the paper is arranged as follows. After introduction, the structure of the X-Y planar motor and θ-*Z* rotary-linear motor is introduced in the second section. Then mathematical background and finite element analysis (FEA) of each axis of motion is performed in the third section. Last, control strategy and corresponding experimental results are provided.

Structure of multi-dimensional SR motors

The X-Y planar motor

The design of direct-drive 2D motor derives from the extension of linear SR motor previously studied (Pan *et al.*, 2009) into two vertical dimensions. The 2D SR motor is based on the "straightened-out" version of two 6/4 pole rotary SR motors along both X and Y directions with "passive-stator-active-translator" motor structure (Krishnan, 2001) employed for both axes of motion. As shown in Figure 3, the prototype of the planar motor consists of the following main parts:

- The stator has an aluminum base with multiple, laminated silicon-steel blocks.

Figure 3 The X-Y planar motor prototype

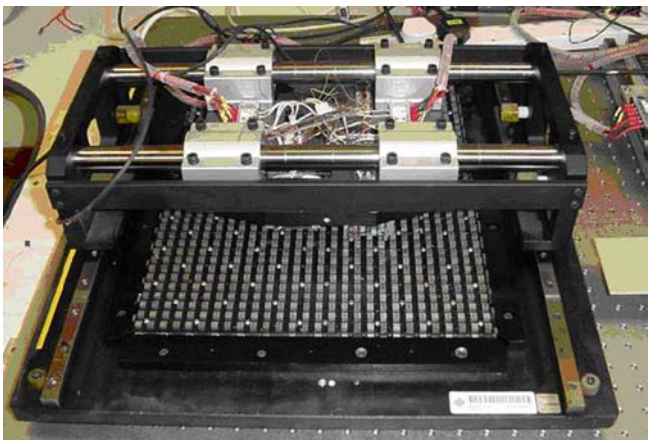

- Six laminated silicon-steel slots are wound with coils with an arrangement that any one slot and its adjacent neighbor are responsible for perpendicular axis of motion.
- Two pairs of supporting mechanical sliding bars hold the moving platform and maintain the air gap and optical encoders are mounted on each moving platform to detect and feedback its real-time position information.

The stator

As shown in Figure 4(a), the stator consists of:

- an aluminum square base;
- a pair of sliding guides for Y-axis of motion;
- stator element matrix; and
- mechanical holding components.

The stator contains multiple laminated silicon-steel blocks held together by epoxy glue. A rigid aluminum base plate is made to support the blocks and ensure enough travel range for the moving platform which reduces the weight and does not affect the magnetic path. The function of the aluminum holding plate is to fix all the stator elements together and ensure that all stator pole extrusions are at the same height.

The stator applies the "LEGO block" idea method (Cheung *et al.*, 2007) for magnetic path circulation and it is constructed from a combination of magnetic bricks. With four-block elements stacked up as one unit, any number of such units can be generated and combined together to form a whole base of any size and dimension as shown in Figure 4(b). This unique stator structure not only reduces eddy currents but also makes mass production and flexible customization available. Therefore, the overall construction complexity and manufacturing cost can be reduced.

The mover

The mover body consists of a set of mover plates laminated together with one excitation coil and six identical mover bodies with two sets of three-phase windings comprise of the moving platform as shown in Figure 5. Coils for perpendicular force generations are arranged in alternation and mounted on the mover slots with wide magnetic teeth. This arrangement facilitates output forces more evenly along the entire moving platform with the following advantages:

- The motor winding scheme is simple and straightforward with the structure of individual mover with winding coil.

Figure 4 Stator structure (part view)

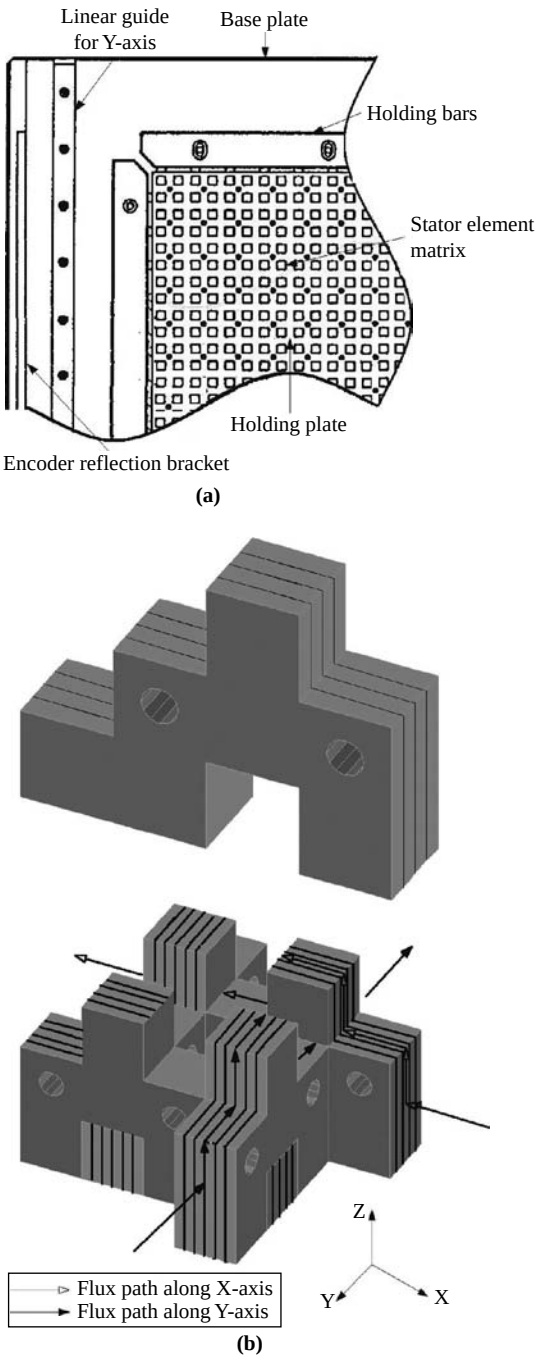

Therefore, the overall manufacture cost and complexity are greatly reduced.

- Zero mutual inductance can be achieved between each adjacent mover with flux-decoupled windings (Liu *et al.*, 1996). The flux-decoupled characteristic between any phases of the mover ensures independent excitation for each mover coil.
- There is no need for reconfiguration of motor structure if the motor is required to travel a different range. The motor can be readily adapted to a new traveling distance with suitable linear guides.

Figure 5 Mover structure

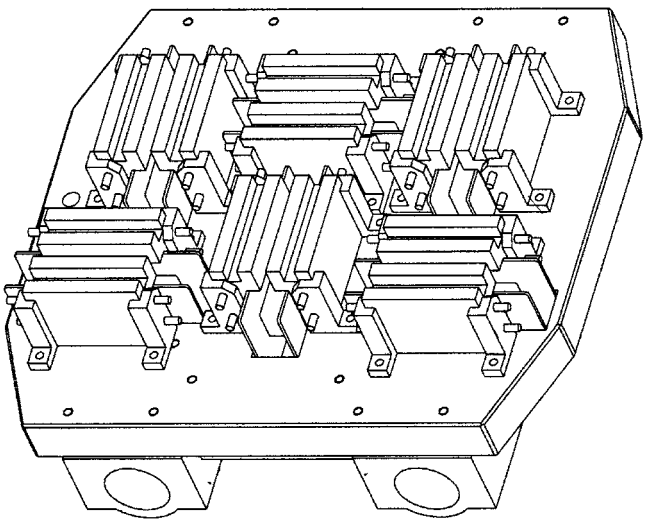

The θ-Z rotary-linear motor

Derived from the above X-Y planar motor, by "wrapping" the planar motor vividly along the two edges together with the moving platform, a cylindrical machine would be formed capable of both rotary and linear motions. Considering manufacture simplicity, the prototype applies the linear stroke within one pole-pitch and rotation as a typical 6/4 SR machine. The overall structure of the rotary-linear motor is shown in Figure 6.

The rotor

The rotor rod has a uniform silicon-steel stacking structure along the rotation axis as that of a rotary SR motor. The stacking utilizes laser soldering instead of long screws to avoid mechanical destruction such as holes and improve the magnetic circuit for a better output performance.

The stator

The stator is composed of three magnetic rings wound with windings as shown in Figure 7. The rotary ring has the typical 6/4 SR motor structure with three-phase windings serially connected (Miller, 1993). Two linear propulsion rings are installed on both sides of the rotary ring to balance translation forces. Both rings have two poles facing oppositely with winding connection in series.

Figure 6 The θ-Z rotary-linear motor

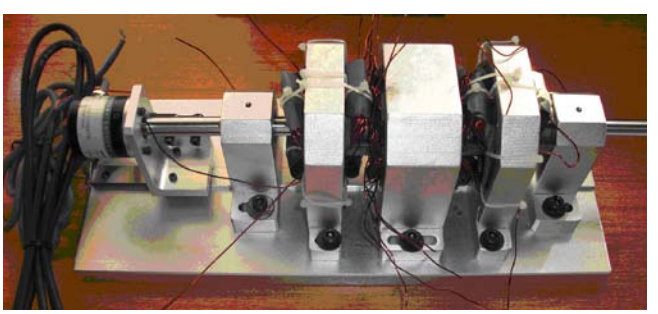

Figure 7 The stator rings

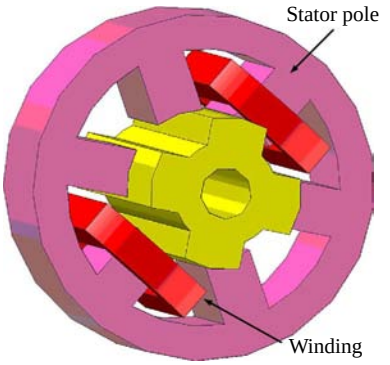

(a)

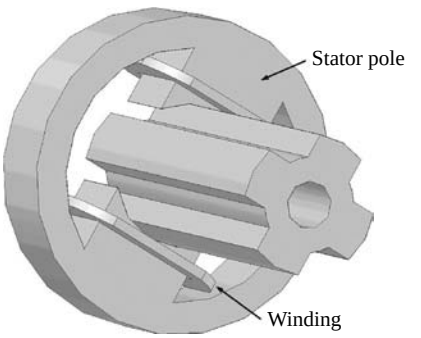

(b)

Notes: (a) The rotation ring; (b) the linear propulsion ring

Characterization of multi-dimensional SR motors

Mathematical formulations

Voltage balance equation

Since each axis of motion is magnetically decoupled, the equation that governs the voltage balance relationship of the SR motors can be described as the following (Miller, 1993):

$$V_k = R_k i_k + \frac{\partial \lambda_k(i_k, x)}{\partial x}\frac{dx}{dt} + \frac{\partial \lambda_k(i_k, x)}{\partial i_k}\frac{di_k}{dt} \tag{1}$$

where V_k, i_k and R_k are winding voltage, current and resistance. $x(t)$ is relative position from the mover or rotor to the stator and λ_k is flux-linkage. The force balance equation can be described as the following for any direction of linear movement as:

$$\begin{aligned} f_{x(y)}(i_a(t), i_b(t), i_c(t), x(t)) &= \sum_{k=a}^{c} \frac{\partial \int_0^{i_k(t)} \lambda_k \cdot d\tau_k(t)}{\partial x(t)} \\ &= \sum_{k=a}^{c} f_k(i_k(t), x(t)) \\ &= M_m \frac{d^2x(t)}{dt^2} + B_v \frac{dx(t)}{dt} + f_l(t) \end{aligned} \tag{2}$$

where $f_{x(y)}$ is generated electromagnetic force, $f_l(t)$ is the load force, M_m and B_v are mass and friction coefficient, respectively.

Torque generation

Torque T_e is presented by equation (3) as:

$$T_e = \mathcal{J}\frac{d^2\theta}{dt^2} + K\frac{d\theta}{dt} + T_L \tag{3}$$

where $\mathcal{J}$ is moment of inertia, K is friction coefficient and T_L, load torque.

Force generation

Since the linear part of the rotary-linear motor is a non-linear electromagnetic device and each ring has identical dimension and ratings, the general representation of force production for any one ring can be described as:

$$F_i = \frac{\partial W_{co}}{\partial x} \tag{4}$$

where force F for the ith linear ring is calculated as the change of co-energy W_{co} according to displacement x. If the current is low and the force is generated under unsaturated region:

$$F_i = \frac{1}{2}\frac{\partial L_i}{\partial x} I_i^2 \tag{5}$$

where L_i is the inductance of ith ring and force is approximately considered as half of change of inductance with x multiplied by current squared, regardless of current direction.

Finite element simulation

To precisely represent the four-axis motion system, 3D finite element models (FEMs) are constructed for each axis of motion using Ansoft Maxwell® software package in order to investigate end and edge effects (Rudnev *et al.*, 2003).

The finite element model

For the X-Y planar motor, the 3D FEM has been constructed with one mover and its closest neighbor to verify that any of the two movers are flux-decoupled. A 3D "cut" vertical to the Z-axis has also been performed along the 3D FEM and a 2D contour plot of flux distribution is derived as shown in Figure 8(b). As can be seen from both the simulation results, magnetic flux merely distributes within the short magnetic path among the mover with its excitation coil at 8A, the stator area and the air gap space between them. This is because the magnetic path between the two adjacent movers has as relatively large reluctance as air.

For the θ-Z rotary-linear motor, the 3D FEM of rotary and linear part are shown in Figure 9. As can be seen from Figure 9(c), the circulation of magnetic path is between the end part of the rod, air gap and the linear propulsion ring.

Flux calculation

Flux-linkage can be investigated from different positions or angles with respective to current levels from FEA for the inspection of magnetic characteristics. For the rotary part of rotary-linear motor, one pair of serially connected coil windings are built for one doubly salient phase since all phases have the same dimension and ratings. Flux-linkage is calculated from different current excitations according to relative angle from the rotor rod to the stator as shown in Figure 10(a). It can be concluded from the results that the magnetic path enters saturated region around 4A.

Flux-linkage for linear movement is calculated as the rod moves along with different relative positions from 0 to 21 mm (0 is fully aligned position and 21 mm, fully un-aligned position). Also only one pair of serially connected coil windings is built and the calculation results are shown in Figure 10(b). Considering one direction of movement (X-axis) for the X-Y planar motor, the 3D flux-linkage profile is derived respective to position and current as shown in Figure 10(c).

Figure 8 FEM verification of zero mutual inductance

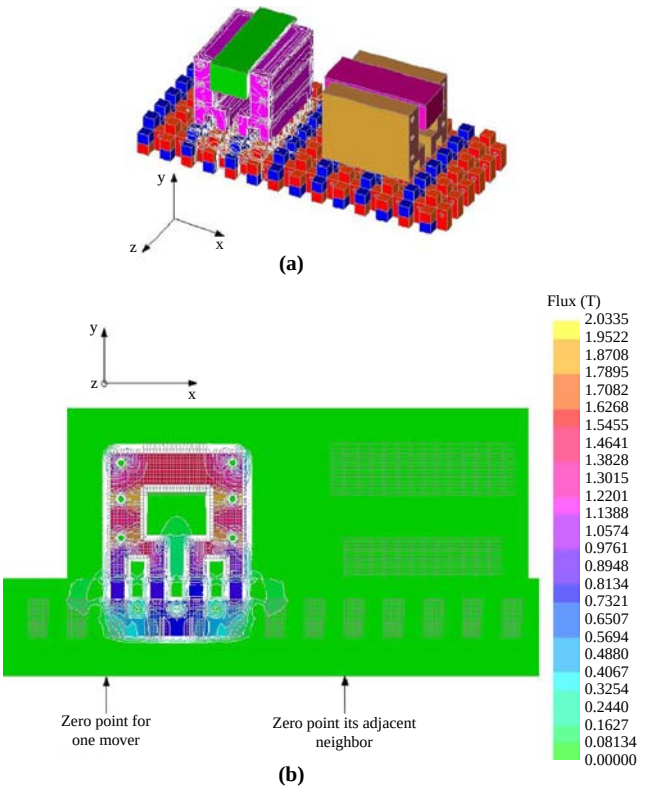

Torque and force calculations

Torque is calculated according to different current excitations with respect to relative positions (Benhama *et al.*, 1999) from the rotor to the stator as shown in Figure 11(a). The torque results also verify saturation effect becomes dominant at 4A. Propulsion force profile according to different positions within one pole-pitch with respect to different current levels is shown in Figure 11(b) for the Z-axis. The calculation curves clearly demonstrate a non-linear relationship between the force and the relative positions according to different current levels. Therefore, a proper linearization scheme will be introduced for position control of the linear part.

Propulsion force for the X-axis is also calculated as shown in Figure 11(c). It can be seen that at lower current excitations, maximum force occur at the position of half pole-teeth (3 or 9 mm) and the waveforms are sinusoid-like curves. At higher current levels, such as 9A or above, the waveforms become distorted that force climbs to peak earlier and the maximum values appear before the mid pole-teeth within one pole-pitch from the fully un-aligned position to fully aligned position. This is because the magnetic materials have entered saturation region and the interaction becomes dominant accompanied by much more end effects.

It can be concluded from the FEA results that the SR motor for each axis of motion demonstrates a highly non-linear relationship of flux-linkage, torque or force respective to position and current. To overcome these non-linear behaviors, suitable decoupling control strategy needs be developed.

Figure 9 3D FEM and flux distribution of the linear part

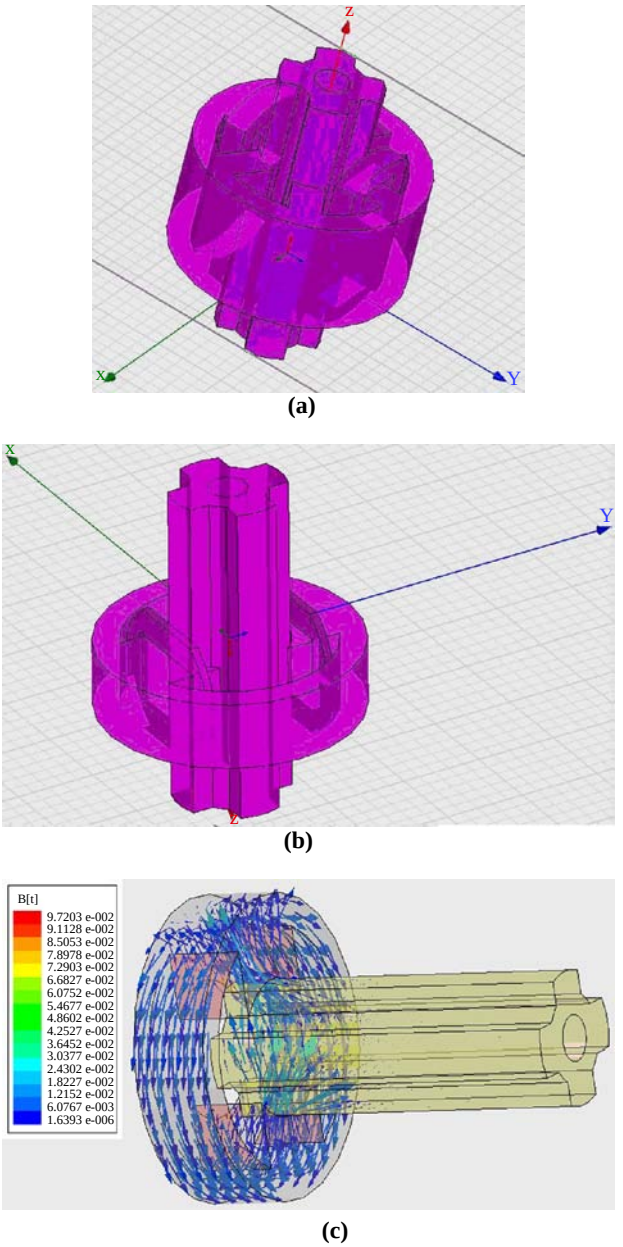

Figure 10 Flux-linkage calculation for (a) rotary part, (b) linear part and (c) X-axis of planar motor

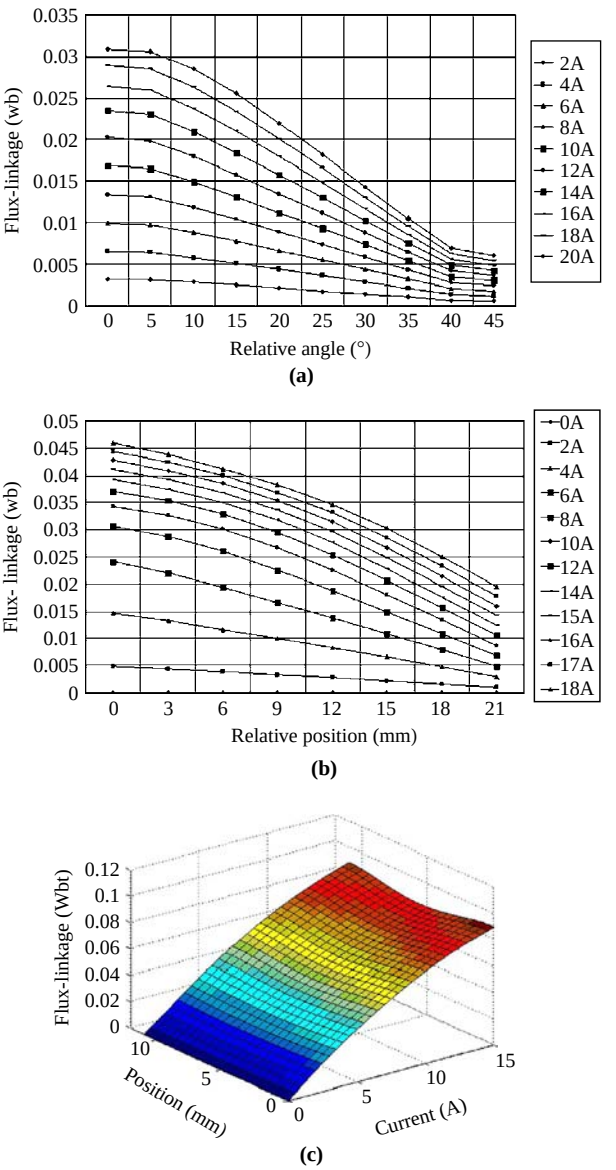

Torque and linear propulsion force measurement

Torque and force measurement is conducted by a torque and a force gauge. A mechanical fixture is installed to divide one pole-pitch into a number of divisions finely enough. An interface circuit has also been built for signal amplification and transfer of sensored voltage output to the A/D channel of the control card. Angle and position information are fed back to the PC from the optical rotary and linear encoders. The various input current excitations are provided with a generalized current driver. When all the signals are ready, they are sampled consequently into the PC for further data processing.

As shown in Figure 12(a), torque reaches peak value at a relative degree of 35, which corresponds with the FEM results. The force measurement for Z-axis results are shown in Figure 12(b). Compared with the simulation results from FEM, the measured data have good correspondence. Force from one of the movers in X-axis of movement is recorded and the result is shown in Figure 12(c), which corresponds with the FEM result. The waveform distortion from saturation effect is also apparent. The main difference between simulation and experimental results prove that under the same current excitation, torque or force output is comparatively smaller than that of FEM. This is mainly due to static frictions from the sliding support and measurement errors.

Control strategy and experimental results

Since each axis of motion from the four-axis machine exhibit a non-linear property, a linearization scheme between torque/force with position and current should be introduced such as

Figure 11 (a) Torque and (b) force calculation from FEM

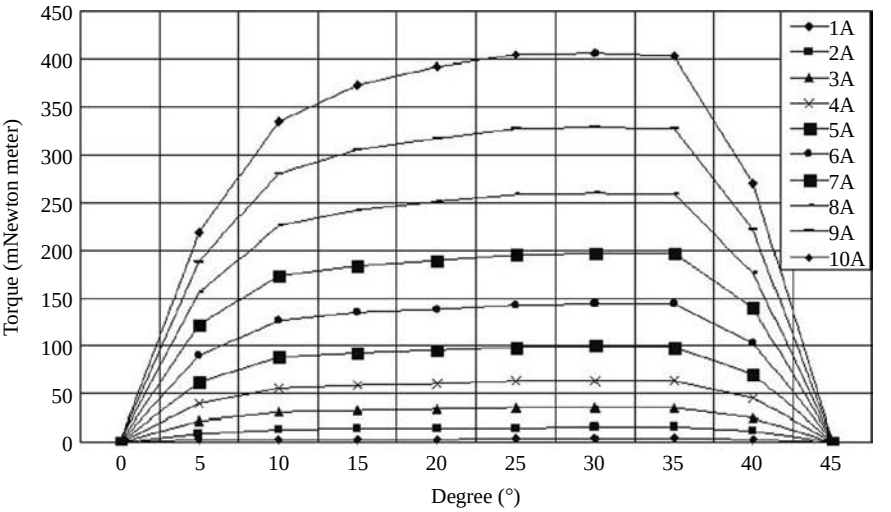

(a)

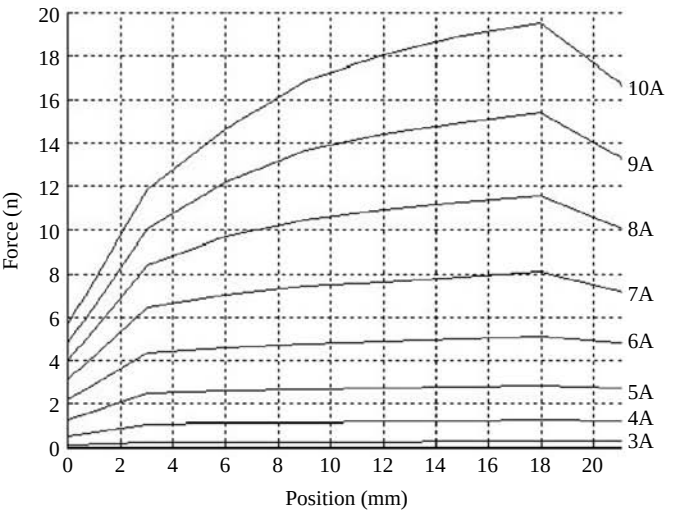

(b)

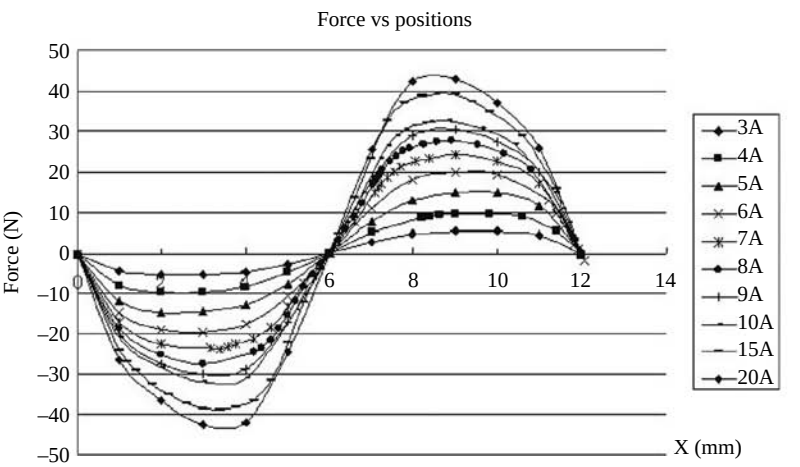

(c)

Figure 12 Torque (a), Z-axis force (b) and Y-axis force measurement results

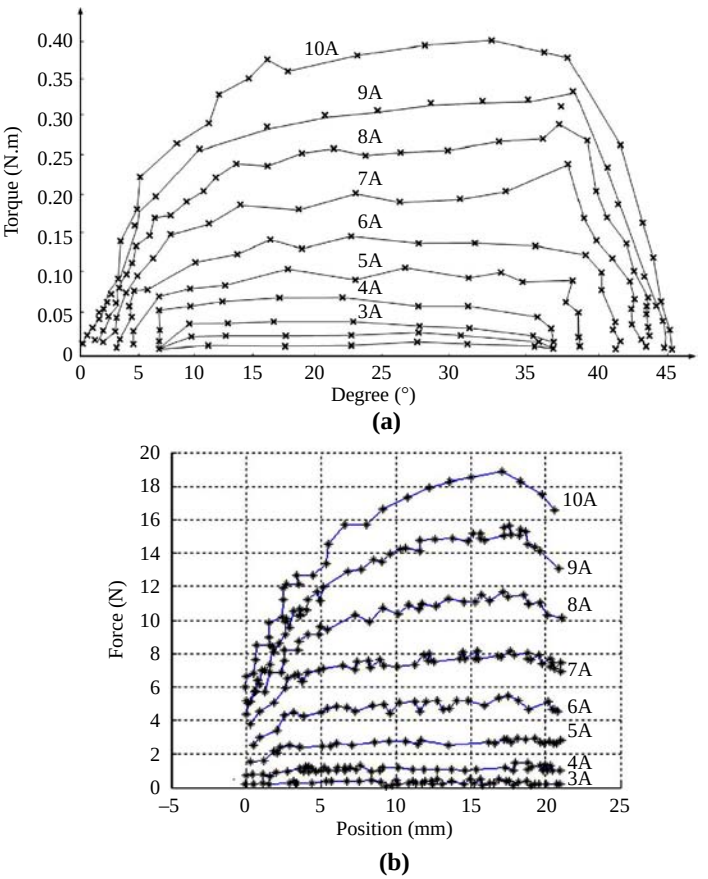

a look-up table. A cascade dual loop control strategy is proposed as the inner digital current loop with a higher sampling frequency and position loop with a slower one. The dual loop cascade controller scheme is based on the assumption that the current controller has accurate tracking capability.

The experiment is implemented on a dSPACE DS1104 DSP motion controller card which has an on-board 250 MHz DSP for real-time computation. It consists of two channels of 24-bits incremental encoder inputs, six channels of 12-bit analog input and six channels 12-bit analog output. The control card can directly interface with Real-Time Workshop and MATLAB and control parameters can be modified online. The overall control block diagram for any two-axis motor is shown in Figure 13 with a sampling rate of 10 KHz for the inner current loop and 2 KHz for the outer position loop.

The position step response of the X-Y planar motor can be found in Pan *et al.* (2005) from previous research work. For trajectory response, the error dynamics for X- and Y-axis can be found in Figure 14(a) and (b). The absolute errors fall within 0.2 mm, 1.2 per cent of the total range (16.56 mm). It is clear that for both diagrams, the errors for opposite directions are not identical in each axis of motion. This is because the mechanical structures in both axes are not uniform such that the motor experiences unbalanced frictions at different positions. It can be seen in Figure 14(c) and (d) that the tracking profiles from each axis of linear motion is capable of following the command signal precisely. Owing to imperfection of mechanical manufacture, performance of each axis of motion is not totally identical. From the above experimental results, the position controllers are capable of correction for such imperfections that exist in mechanical manufacture.

Conclusion

The proposed four-axis machine based on direct-drive, 2D SR motors described in this paper has a simple and robust structure. Based on simulation and experimental results, each axis of motion is capable of high-performance operation under appropriate control strategy. However, due to inevitable mechanical imperfections, more research work concentrating on advanced control algorithms such as robust or adaptive control scheme is suggested to be carried out to correct the asymmetry from position response and improve control precision. Research work based on design and optimization of motor structure is also expected in future. Considering the performance from the prototype, it is expected to find applications in low-level force and torque output such as automated small-scale PCB drillings. The authors also believe that with the development of direct-drive machines and technology, new trend of manufacture can be fulfilled with high-performance, low-cost direct-drive facilities.

Figure 13 Control scheme for two-axis SR motor

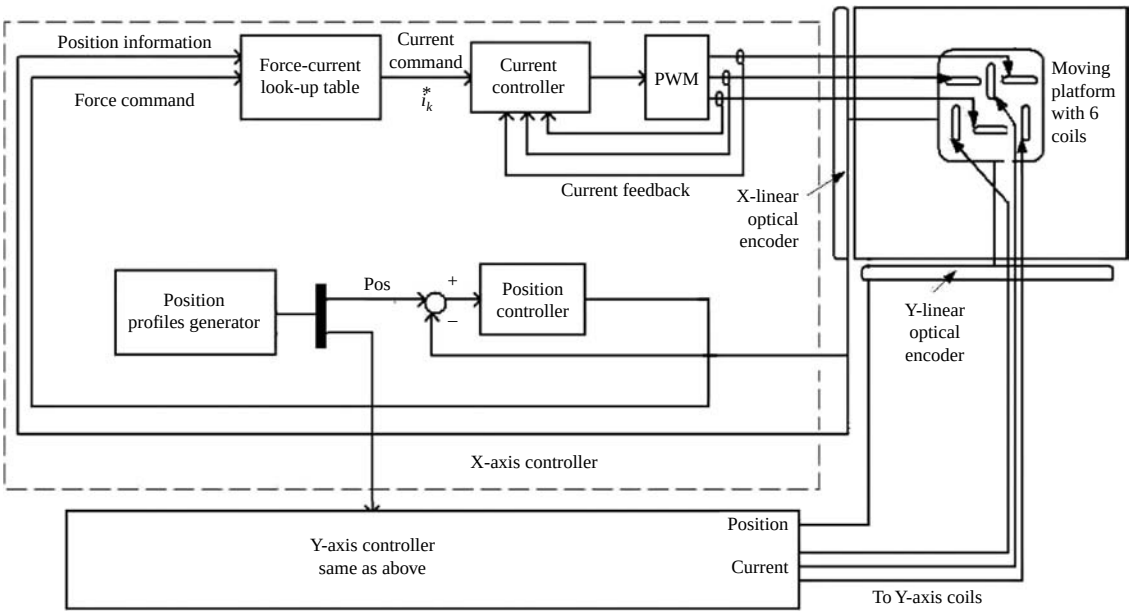

Figure 14 Overall performance and performance of the Z-, X- and Y-axis motor

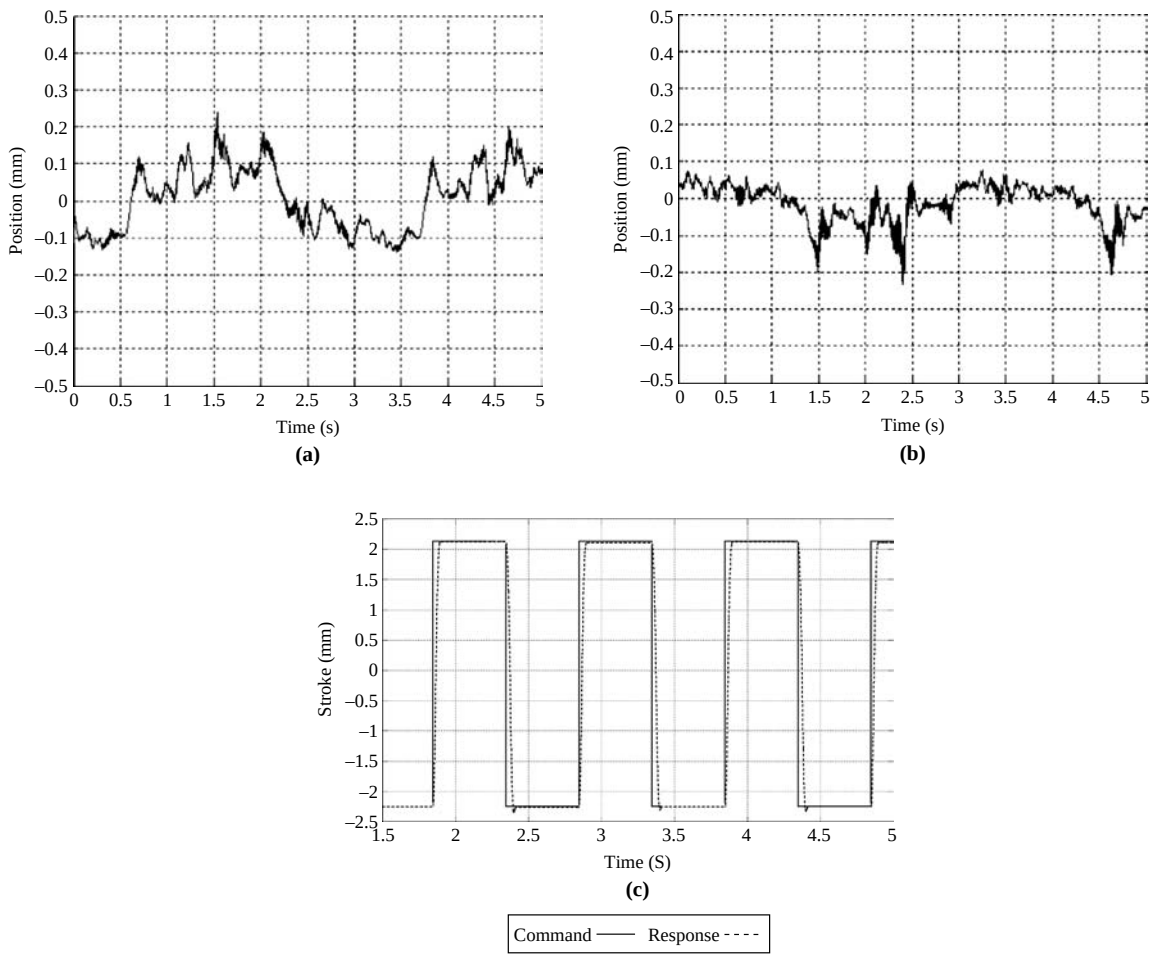

References

Benhama, A., Williamson, A.C. and Reece, A.B.J. (1999), "Force and torque computation from 2-D and 3-D finite element field solutions", *Electric Power Applications, IEE Proceedings*, Vol. 146 No. 1, pp. 25-31.

Cheung, N.C. and Pan, J.F. (2003), "Using variable-reluctance actuators in automated manufacturing machines", *International Journal on Industrial Robot*, Vol. 30 No. 4, pp. 355-62.

Cheung, N.C., Pan, J.F. and Yang, J.M. (2007), "Two-dimensional variable reluctance planar motor", US Patent No. 7,170,203.

Krishnan, R. (2001), *Switched Reluctance Motor Drives: Modeling, Simulation, Analysis, Design, and Applications*, CRC Press, Boca Raton, FL.

Liu, C.T., Chen, L.F., Kuo, J.L., Chen, Y.N., Lee, Y.J. and Leu, C.T. (1996), "Microcomputer control implementation of transverse flux linear switched reluctance machine with rule-based compensator", *IEEE Transactions Energy Conversion*, Vol. 11, pp. 70-5.

Miller, T.J.E. (1993), *Switched Reluctance Motor and Their Control*, Oxford University Press, London.

Pan, J.F., Cheung, N.C. and Yang, J.M. (2005), "High-precision position control of a novel planar switched reluctance motor", *IEEE Transactions on Industrial Electronics*, Vol. 52 No. 6, pp. 1644-52.

Pan, J.F., Cheung, N.C., Cao, G.Z. and Lin, L.M. (2009), "Design and analysis of a DSP-based linear switched reluctance motor", paper presented at the 3rd International Conference on Power Electronics Systems and Applications, Hong Kong.

Rudnev, V., Loveless, D., Cook, R. and Black, M. (2003), *Handbook of Induction Heating*, Marcel Dekker, New York, NY.

Corresponding author

Norbert Cheung can be contacted at: Norbert.cheung@polyu.edu.hk